Available online at www.sciencedirect.com
ScienceDirect
Catalysis Today 120 (2007) 54–62
CATALYSIS TODAY
www.elsevier.com/locate/cattod

Engineered SMR catalysts based on hydrothermally stable, porous, ceramic supports for microchannel reactors

Bradley R. Johnson *, Nathan L. Canfield, Diana N. Tran, Robert A. Dagle, X. Shari Li, Jamelyn D. Holladay, Yong Wang *

Pacific Northwest National Laboratory, P.O. Box 999, Richland, WA 99354, USA

Available online 11 September 2006

Abstract

A novel engineered, porous, ceramic, catalyst support for stable, high temperature (>800 °C) steam methane reforming operation was demonstrated with a rhodium catalyst. The support was designed for operation in microchannel reactors. Typically high temperature alloys such as FeCrAlY or 600 series nickel-based alloys are used as structural supports that are wash-coated with catalyst-impregnated, high surface area, ceramic powders. The hydrothermal conditions used for methane steam reforming create several material challenges that interfere with the performance of metallic supports: corrosive degradation of the metal, delamination of the wash-coated catalyst from the metal support, and accelerated sintering of the high-surface area ceramic powder used to disperse the metal catalysts. Additionally, undesirable side reactions such as coke formation promoted by the support metal typically necessitate operating SMR reactions at higher than equilibrium steam to carbon ratios. The engineered, porous, ceramic support with Rh catalyst was tested at a steam to carbon ratio of 1:1, a contact time of 27 ms, and temperatures up to 900 °C. Near equilibrium conversion and selectivity were achieved. It was found that there was no degradation or sintering observed in the engineered, porous, ceramic support, the catalyst did not delaminate from the support, nor was any coke formation detected after 100 h time-on-stream (TOS) under these reaction conditions.

Keywords: Methane steam reforming; Microchannel reactors; Engineered catalyst; Hydrothermally stable catalyst

1. Introduction

Microchannel reaction technology is designed around a paradigm of building reactors that consist of multi-layer, high aspect ratio, closely spaced (<1 mm) channels [1]. The objective is to minimize heat and mass transport distances so as to maximize efficiency. Microchannel reactors can have heat transfer rates as high as 35,000 W/m^{2}K compared to 100–700 W/m^{2}K for conventional reactors [2]. When applied to a wide variety of chemical reactions, significant reduction in reactor and system volume can potentially be achieved while maintaining high throughput. Kinetically limited reactions typically do not show the same improvements due to heat transfer enhancement, but can benefit from improved temperature control.

For over a decade, we have developed microchannel reactors for various applications. Some of the applications include fuel vaporization [3,4], water-gas-shift and reverse water-gas-shift reactions [5,6], steam reforming [1,6–13], heat transfer [3,4,14], mass transfer [15], catalytic combustion [4,14,16], partial oxidation [17] and gas-to-liquid processes [18]. In each application, the microchannel architecture decreases the device volume by over an order of magnitude compared to conventional technology at the same throughput.

Development of microchannel reactor technology was advanced by decoupling the reactor design from catalyst development and application by using thin shims as catalyst supports that could be inserted into the microchannels [1]. Two of the key technologies required for successful support shim development are catalyst adhesion and corrosion protection. Active catalysts are typically impregnated into high surface area metal oxide powders that act as carriers to disperse the metal catalysts. The carrier powders are typically applied to the support shims by wash coating (dipping the shims in an aqueous slurry of ceramic powders that were previously impregnated

* Corresponding authors. Tel.: +1 509 372 1635; fax: +1 509 376 3108.
E-mail addresses: Bradley.johnson@pnl.gov (B.R. Johnson), yongwang@pnl.gov (Y. Wang).

0920-5861/$ – see front matter © 2006 Elsevier B.V. All rights reserved.
doi:10.1016/j.cattod.2006.07.056

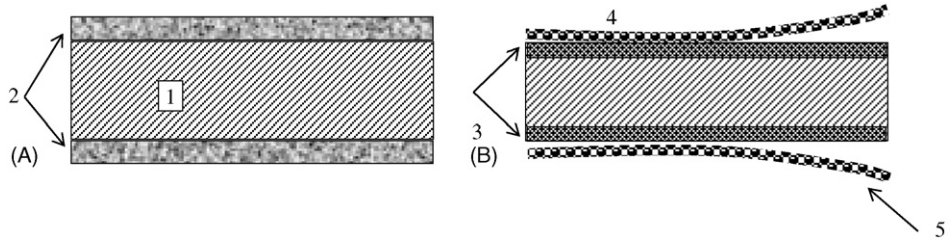

Fig. 1. Illustration of the cross-section for a metal-based support used as in insert in a microchannel reactor. (A) The center section (1) represents the metal support, and the outer layers (2) represents the wash-coated engineered catalyst that is composed of a high surface area, porous, ceramic, carrier powder impregnated with a metal catalyst. (B) After exposure to hydrothermal conditions, the support metal experiences corrosion (3), the catalyst carrier powders sinter (4), and they can also delaminate from the support metal (5).

with the active catalyst) [2]. The use of small-gap channels necessitates the use of very thin support shims, thereby aggravating the corrosion problem. Corrosion resistance has been addressed by using support shims made from oxide dispersion alloys such as FeCrAlY or high nickel-based alloys and by applying a protective barrier coating to these inserts [2]. However, the performance is contingent upon the integrity of the coating. Examples that illustrate the material challenges associated with catalyst adhesion and corrosion are shown in Fig. 1.

Steam methane reformation (SMR) is an industrially significant chemical process, with potentially increased economic value in light of the need for a hydrogen-based fuel economy. The chemical reaction for this process is shown in Eq. (1). Since the SMR reaction is highly endothermic, microchannel reactors can be particularly effective [19]. Successful performance of an SMR reactor is contingent not only upon the design of the reactor, but also upon the development of a highly active, selective, and stable catalyst that will fully utilize the reactor's heat and mass transfer capability [2]. Therefore catalysts tailored to microchannel architecture are needed:

$$CH_4 + H_2O \leftrightarrow 3H_2 + CO \quad \Delta H = 250\,\mathrm{kJ/mol\,at\,20\,^{\circ}C} \qquad (1)$$

This endothermic reaction is thermodynamically favored at high temperatures and low pressures. Typical operating conditions are between 800 and 900 °C at pressures between 1 and 25 bar, with steam-to-carbon (S:C) ratios typically close to 3. Undesirable side reactions (promoted by the metal alloys used to support engineered catalysts) tend to result in coke formation, thus necessitating higher than equilibrium S:C ratios. The need to use extra water to prevent coke formation presents an additional energy burden and increases operational costs.

There are several material challenges associated with the operating conditions required by this chemical process. The combination of steam and elevated temperatures required for this reaction creates a highly corrosive, hydrothermal environment that is capable of rapidly degrading even advanced high-nickel content and corrosion resistant alloys used as catalyst support shims. These hydrothermal conditions also cause sintering of high surface area and metal oxide powders (e.g. gamma alumina) used as carriers for dispersing active platinum group metal catalysts. Sintering of the carrier powder leads to deactivation of the catalyst. Additionally, delamination of the ceramic carrier powders from metal supports has been observed after prolonged operation. This may have been due to corrosion at the metal support–wash coat interface, or thermal expansion mis-match issues. Consequently, the integrity of the metal supports, the stability the ceramic carrier powder, and its adhesion to the metal support are all degraded by the operating conditions necessitated by this reaction (Fig. 1). These issues present significant materials challenge to the design and development of long-life SMR microchannel reactors.

The material challenges along with the operational challenges of coke formation at low S:C ratios, prompted an investigation to develop solutions. Using the same paradigm of a shim insert as the catalyst support, the goal of this research was to develop a materials solution to the challenges of support corrosion, catalyst adhesion (delamination), and catalyst deactivation due to carrier powder sintering. Consequently, a porous ceramic material based on alpha alumina was developed to serve as the support for the precious metal catalyst that could be inserted as a shim into a microchannel. The use of highly stable alpha alumina as the support addresses the problems of corrosion in the support and sintering of meta-stable carrier powders. The use of alumina as the support also eliminates deleterious coke forming side reaction promoted by metal supports. Also, since the catalyst was directly applied to the support, the problem of carrier powder delamination was eliminated. Rhodium was chosen as the catalyst for this system due to its excellent SMR performance [20]. The engineered and ceramic-based catalyst was tested under aggressive SMR conditions to evaluate its potential advantages for the use in microchannel reactors.

2. Experimental

Porous ceramic support shims were fabricated from alpha-alumina powder (Alcoa A16 Super Grind®) using an aqueous tape cast process [21]. The tape casting processing variables such as the binder and plasticizer system, the cast tape thickness, drying parameters, binder burnout schedule and sintering schedule were optimized to produce a porous, flat, thin, ceramic support suitable for insertion into a microchannel reactor. The density and porosity of the support shims were determined using Archimedes method [22]. Specific surface area (SSA) measurements on the shims were made using

nitrogen gas adsorption experiments. Their microstructure was characterized using scanning electron microscopy (SEM, JEOL 5900). Particle sizes and pore sizes were manually measured from digital micrographs by drawing line segments on a minimum of 100 particles (50 pores) using the software package Digital Micrograph® by Gatan. Sintering studies were done on green tapes to determine the amount of shrinkage in *X*, *Y*, and *Z* directions during firing for a given degree of porosity. Support shims were laser cut from green tapes such that the final, post-sintered dimensions would meet the high dimensional tolerances for microchannel testing.

The support shims were cleaned by sonicating them in ethanol for 5 min to remove any potential contaminants. They were then dried and calcined by heating at 5 °C/min with a hold at 110 °C for 2 h and another hold at 500 °C for 2 h. This same heat treatment schedule was used for all subsequent calcination steps. Catalysts were applied to the shims by soaking them in an acidic solution of $Rh(NO_3)_3$ (Alfa Aesar, 13.82 wt.% Rh in HNO_3) followed by drying and calcination. Various catalyst loadings were obtained by varying the concentration of Rh in the solution, and the number of soaking and calcination cycles. The catalyst loading was calculated by measuring the weight gain of the shims after dispersing Rh. The amount of weight gain was attributed to Rh_2O_3 and catalyst loading was calculated on a metals basis only. The morphology of the ceramic supports and distribution of the Rh catalysts on them were characterized using an SEM (JEOL 5900) in both secondary and backscattered electron (BSE, Robinson Series 6 detector) imaging modes. Energy dispersive spectroscopy (EDAX Genesis®) was used to verify the identity of the different phases. Transmission electron microscopy (TEM, JEOL 2010F) coupled with EDS (Oxford INCA®) was used in bright field and scanning modes to determine the chemical identity of the observed features, and more accurately characterize the morphology of the Rh.

Catalytic performance of the shims was evaluated in a microchannel configuration by inserting two catalyst-coated ceramic shims into a 51 mm long cylindrical Inconel® 625 rod with a longitudinal slit cut in the center of it that was 0.89 mm wide and 9.4 mm tall. A narrow inert shim of FeCrAlY material felt (Porvair, Henderonville, NC), with a dimension of 250 μm × 2.54 mm × 51 mm, was centered between the catalysts to push them in contact with the channel walls. The microchannel assembly was placed within a clam-shell tube furnace to provide the required endothermic reaction heat. A mixture of methane and water with a stoichiometric steam-to-carbon ratio of 1:1 (molar) and a contact time of 27 ms were used for catalytic testing. Contact time is defined as the catalyst bed volume (total volume of microchannel slot-shims plus gap) divided by the volumetric inlet gas flow rate at standard temperature and pressure. Water was fed into a microchannel vaporizer using an Acuflow Series III HPLC pump. The feed was vaporized at 300 °C and mixed with methane before being introduced to the reactor. Methane was controlled using a Brooks 5850E mass flow controller. Inconel® sheathed type K thermocouples were used for temperature measurement in the catalyst bed, preheating zone, vaporizer and outlet. A condenser and desiccant bed were used to remove water from the product stream. The dry gaseous effluent was analyzed using a MTI gas chromatograph (Model Q30L) equipped with MS-5A and PPQ columns and a thermal conductivity detector (TCD).

3. Results and discussion

Alpha alumina was chosen for use as the support material for this application because of its superior durability under the inherently corrosive environment characteristic of SMR reaction chemistry. However, bulk monolithic and ceramic materials were not suitable for this application due to the narrow dimensions involved with microchannel reactor design. Consequently, ceramic tape cast processing was chosen as the preferred method to produce high tolerance, flat, thin, porous ceramic support shims. The various processing parameters used to create the porous ceramic support shims were engineered to optimize three key properties: (1) a microstructure that contained a high degree of porosity to facilitate the catalyst impregnation and the accessibility of reactant gas molecules, (2) sufficient strength for durability during handling and testing, and (3) durability under SRM reaction conditions. Tabulated data of relevant physical properties of the support shims is shown in Table 1.

The morphology and microstructure of the engineered, porous, alpha alumina ceramic support shims is shown in Fig. 2. Macroscopically, the support shims appeared opaque and solid. However, due to the sub-micron sized powders used to make them, and the process conditions by which they were made, they actually contained approximately 50 vol.% interconnected porosity. The structural strength for the support is derived from the formation of necks between the particles that formed during the sintering step. The microstructure as shown in Fig. 2B was projected to be suitable for a catalyst support for two main reasons. First, the high degree of open porosity provides high surface area for catalyst dispersion as well as good accessibility to gas phase reactants, and second, the high degree of connectivity between the particles should provide adequate strength for handling. Control of the sintering process was crucial to obtain the optimized microstructure shown in Fig. 2B.

Two engineered catalysts containing different weight loadings of Rh were prepared using the porous ceramic support shims described above. The first set of shims, designated as S1, contained 10 wt.% Rh, while the second set of support shims (S2) contained 3.7 wt.% Rh. The objective was to determine the effect of catalyst loading on the microstructure of the engineered porous ceramic support

Table 1
Physical properties of engineered, porous, ceramic support shims

Dimensions (mm)	9.4 × 50.8
Thickness (μm)	250
Density (g/cm^3)	1.927
Open porosity (%)	50.7
SSA (m^2/g)	4.88

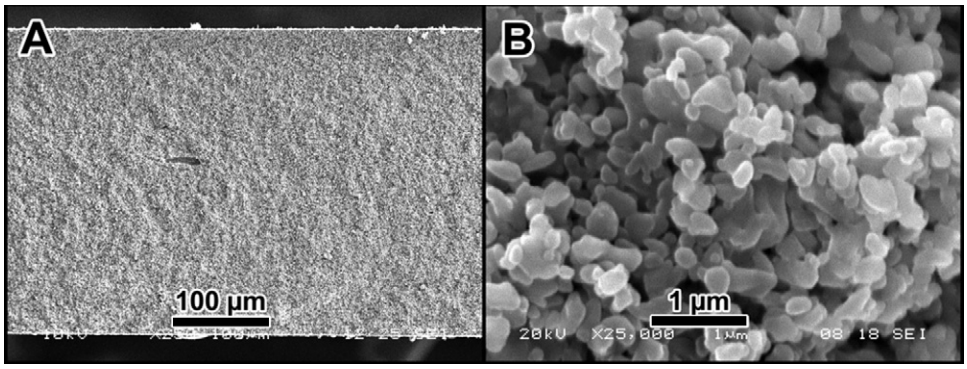

Fig. 2. SEM micrographs from the fracture surface of an aqueous tape cast porous alumina shim.

Table 2
Data on Rh catalyst loading on porous alumina support shim

Specimen	Rh (mg)	Rh (mg/cm^2)[a]	Rh (wt.%)[a]
S1	21.90	4.49	10
S2	8.15	1.71	3.7

[a] Based on the BET surface area and weight of the shim.

shims, and then to correlate that microstructure to their activity and catalytic performance. The catalyst loading data for the two sets of ceramic support shims are summarized in Table 2.

The performance of an engineered catalyst is governed by its microstructure. Thus, the microstructures of these catalysts were evaluated before and after SMR testing to determine impact of the harsh hydrothermal conditions on the microstructure and then to subsequently correlate these changes to their performance. The porous alumina support as well as the Rh catalyst particles were analyzed in detail to look for microstructural changes. Micrographs of S1 shims taken with SEM and TEM prior to testing (after dispersing with the Rh catalyst and calcination, but prior to reduction), and then after catalytic testing under SMR conditions for 100 h time-on-stream (S:C = 1, 27 ms contact time, 1 atm, 900 °C) are shown in Fig. 3. Although unprotected metal supports are susceptible to severe oxidative degradation under such harsh conditions, the microstructure of the porous alumina support was relatively unaffected. Quantitative stereological measurements were made of the alumina particles and pore sizes of the support

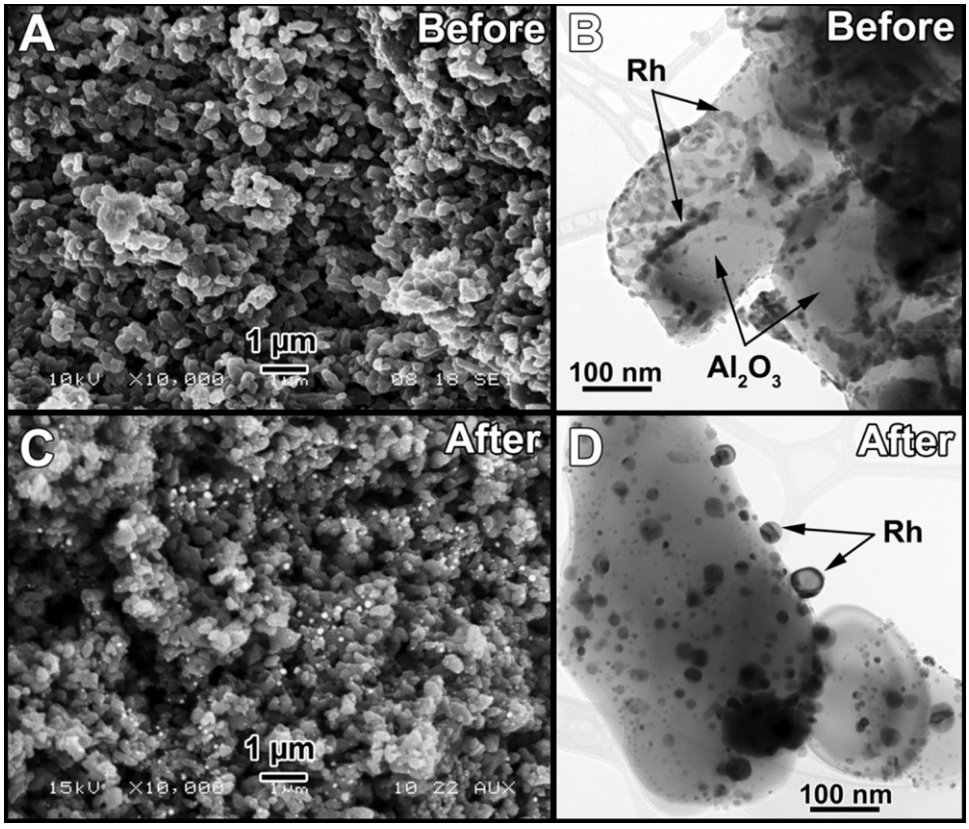

Fig. 3. SEM (A and C) and TEM (B and D) micrographs from specimen S1 (10 wt.% Rh). Micrographs (A and B) were taken after applying the Rh catalyst, but prior to testing, and (C and D) were taken after catalytic testing.

Table 3
Microstructural characterization of tape cast, porous, alumina support before and after catalytic testing

	Al_2O_3 particles		Pores	
	Average diameter (nm)	Standard deviation (nm)	Average diameter (nm)	Standard deviation (nm)
As-made	219.9	62.8	329.2	115.2
After 100 h TOS at 900 °C, S:C = 1, 1 atm	251.6	87.6	357.0	170.8

before and after testing. Only a slight increase in the average particle and pore size was measured, as shown in Table 3. However, the increase in size was less than the standard deviation of the measurement, and thus was within the margin of error. Consequently, this data demonstrates that the porous alumina support was hydrothermally stable under these reaction conditions, and therefore validates it as a candidate support material for this type of application.

Even after close comparison via SEM of Fig. 2B (bare ceramic support) to Fig. 3A (ceramic support with Rh after calcination), it was not possible to determine the presence of discrete Rh particles on the surface of the ceramic support. More detailed examination using a TEM (Fig. 3B) was required to characterize the morphology and spatial distribution of Rh on the ceramic support. The gray scale images observed in TEM bright field (BF) micrographs rely on contrast mechanisms due to diffraction effects of oriented crystals in a coherent electron beam, as well as due to scattering and absorption losses related to atomic mass and specimen thickness (mass-thickness) [23]. Thus, Rh will typically appear darker than alumina (of comparable thickness) in TEM BF micrographs due to its higher atomic number, so long as neither crystal phase is oriented in a diffracting condition. Additionally, EDS analysis was done to confirm the chemical identity of the different phases observed. Thus, in Fig. 3B, the larger, lighter, rounded objects were identified as the alumina grains that composed the ceramic support, while the darker material that appears as a somewhat disconnected coating was determined to be the Rh particles. The irregularly shaped Rh globules had an approximate size of 12–13 nm. It is important to point out that at this stage of the sample treatment, the Rh was still in an oxidized state. It was concluded that the Rh oxide appeared to be somewhat wetting to the alumina surface. A more preferable microstructure would be to have a better dispersion of Rh across the surface of the alumina grains.

After catalytic testing for 100 h at 900 °C, there was a dramatic change in the morphology and spatial distribution of the Rh. Prior to performing the catalytic tests, the catalysts were heated up under a reducing atmosphere to convert the Rh oxide to metallic Rh. The effect of 100 h TOS of SMR testing resulted in sintering of the Rh particles, which is clearly evidenced in Fig. 3C and D. In the SEM micrograph (Fig. 3C), the prominent, small, white spheres were identified as metallic Rh using EDS.

In an SEM, one of the prominent contrast mechanisms is due to differences in average atomic number density. Higher average atomic number species appear brighter than lower average atomic number species because they have a higher yield of back scattered electrons [24]. BSE detectors are designed to take advantage of this phenomenon, thus images obtained from them emphasize atomic number contrast. Consequently, Fig. 3C was taken in BSE mode to facilitate imaging the Rh particles. (No improvement was observed in using BSE imaging in the SEM to look for the Rh for the pre-tested S1 catalysts, as shown in Fig. 3A, due to their dispersion and oxidized condition). Besides atomic number contrast, in an SEM, features can also appear brighter due to an enhanced yield in secondary electrons produced from edge effects [24]. Consequently, the small, discrete, Rh catalyst particles appeared very bright in the SEM due to both their higher atomic number (as compared to the ceramic support), and their spheroidal morphology, and thus are readily imaged even down to nanometer scale sizes. In the TEM BF micrograph (Fig. 3D), however, the Rh metal catalyst particles in general appeared darker than the alumina grains due to atomic mass related scattering losses (exceptions were noted due to variations in relative thickness and/or diffracting particles of either material). Definitive identification of individual particles was determined by EDS analysis, however, and not merely by variations in gray scale intensities. The significant change was that after catalytic testing, the Rh was no longer present as an irregular globular coating, but as discrete crystallites that were sitting on the surface of the alumina grains. In fact, after close observation, some of the Rh crystallites appeared to have hexagonal facets, which may suggest that it had crystallized in an oriented fashion on the alumina surface.

Elemental dot maps were collected of catalytically tested S1 specimens using scanning transmission electron microscopy (STEM) and EDS to further verify and distinguish the Rh particles from the alumina grains. The results are shown in Fig. 4. The STEM BF micrograph in Fig. 4A shows an ensemble of alumina particles coated with Rh where the contrast was a function of diffraction and mass-thickness. Micrographs in Fig. 4B, C, and D shows the spatial distribution and relative concentrations of aluminum, oxygen, and rhodium atoms, respectively. These micrographs were taken by scanning the electron beam across the field of view while collecting EDS spectra at each point so as to form a data cube of spectral intensities correlated to the x–y position of each pixel. The cumulative spectra are then summed, and the relative concentrations of each element are displayed as relative intensities. Thus in Fig. 4B, the bright red areas correspond to high concentrations of aluminum and in Fig. 4C the blue areas correspond to areas of high oxygen concentration. Where there is registry between these images, one can conclude that the features so colored were aluminum oxide – the ceramic support. However, in Fig. 4D, the bright green areas correspond to regions with high Rh content, and can thus be identified as Rh particles. This series of micrographs unambiguously identifies the size, location and spatial distribution of the Rh catalyst on the ceramic support grains, and thus eliminates any potential confusion over the different contrast mechanisms for TEM BF images.

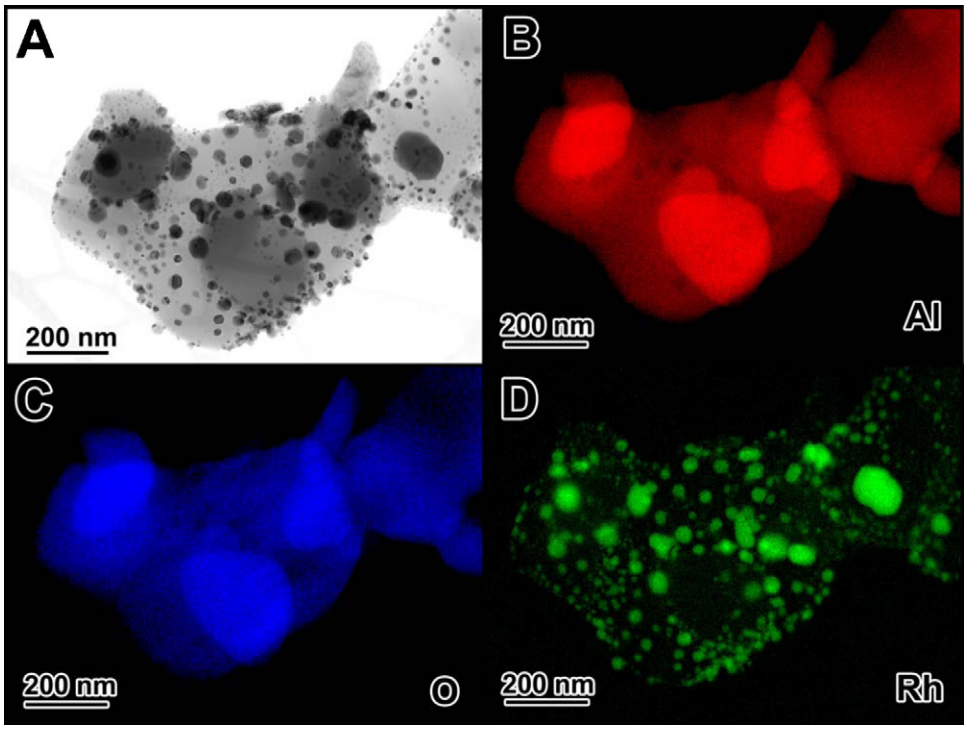

Fig. 4. STEM EDS dot maps of catalytically tested specimen S1.

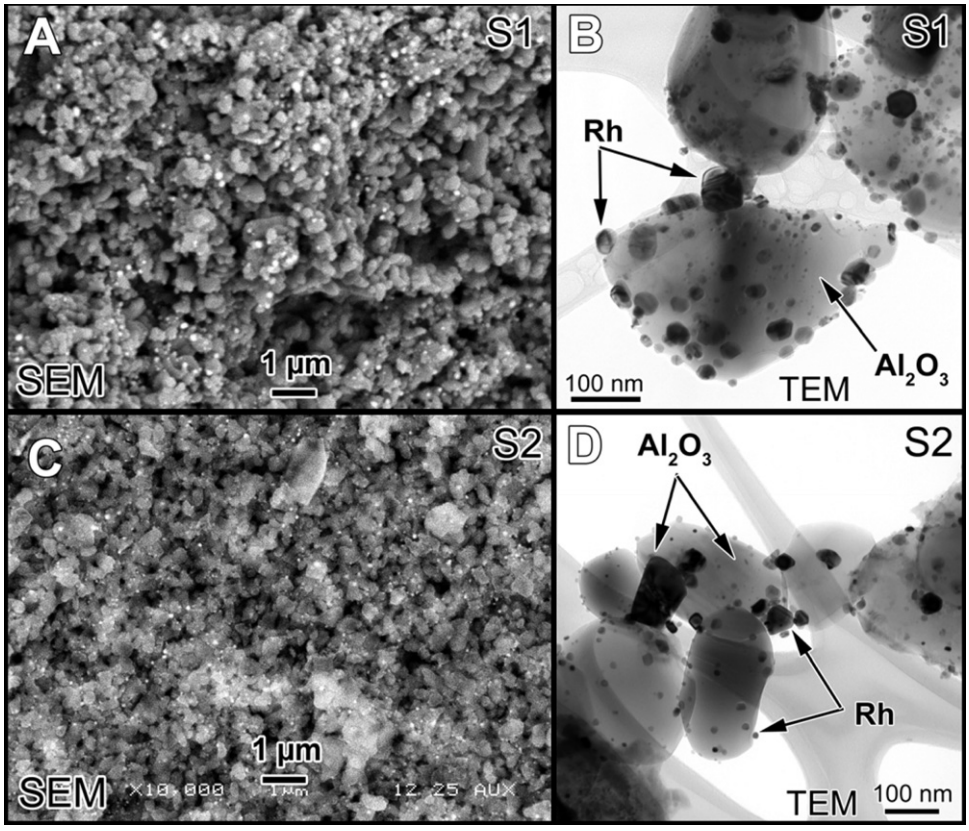

Fig. 5. Microstructural comparison of S1 (A and B) and S2 (C and D) engineered, porous, ceramic supports after catalytic testing. SEM micrographs are shown in (A and C), while (B and D) are the accompanying TEM bright field micrographs.

The microstructure of the S2 specimen was also characterized after catalytic testing under identical SMR conditions as the S1 specimens (100 h TOS, 900 °C, S:C = 1.0, contact time = 27 ms). A comparison of the microstructures of these two specimens is provided. Fig. 5A and B are the SEM and TEM micrographs from the S1 specimen, while Fig. 5C and D are the SEM and TEM micrographs from the S2 specimen, respectively. The contrast mechanisms for the SEM and TEM micrographs are as explained earlier. There were two prominent microstructural difference observed between the two specimens: the size and the concentration of Rh particles were greater on the S1 specimen. This is not only observable qualitatively examining either the SEM and TEM micrographs, but also by stereological measurements as well. These findings were consistent with expectations, since the S1 specimen contained approximately three times the catalyst loading. Detailed stereological measurements were taken from TEM BF micrographs of approximately 150 Rh particles for each specimen. The results and relevant statistics are shown in Table 4. In summary, the Rh particles on the S1 specimen were approximately 56.7% larger in diameter than those on S2. This corresponds to almost 300% greater volume per Rh particle for the spent S1 catalyst. It is possible that surface diffusion under the high temperature conditions of SMR testing, coupled with a greater number of Rh catalyst particles facilitated increased sintering of the Rh catalyst on S1.

As previously stated, the testing parameters used to evaluate the performance and catalytic activity of these two catalysts were a molar S:C ratio of 1:1, a contact time of 27 ms, at a pressure of 1 atm and temperatures up to 900 °C for 100 h TOS. Methane conversion and CO selectivity were measured as a function of temperature during light-off, and the results are plotted in Fig. 6. Extended performance was also evaluated as a function of time-on-stream at a temperature of 900 °C, and the results are shown in Fig. 7. It is interesting to note that the performance of these engineered porous ceramic support shims compares favorably to other metal-based support shims that have been previously reported [20].

As can be seen in Figs. 6 and 7, both catalysts had very high activity under the chosen reaction conditions, and performed similarly. Catalyst S2 had a slightly higher CH_4 conversion and CO selectivity as a function of temperature than S1. The time-on-stream performance of S2 was also better than that of S1. Even though these catalysts were operating close to thermodynamic equilibrium, under the chosen operating conditions, a slight degree of deactivation was observed for both catalysts after 100 h time-on-stream (TOS), with S2 deactivating at a slower rate than S1.

Table 4
Rhodium particle size data for catalytically tested specimens S1 and S2

Specimen	Mean diameter (nm)	Standard deviation	Minimum size (nm)	Maximum size (nm)
S1	19.57	12.30	3.55	84.12
S2	12.49	9.34	2.48	60.22
Δ%	+56.7%	+31.7%	+43.1%	+39.7%

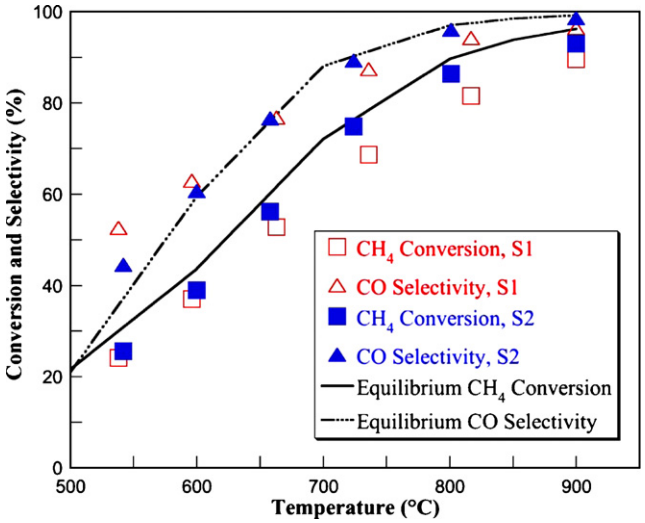

Fig. 6. Methane conversion and CO selectivity for engineered Rh-porous alumina catalytic shims; S1 = 10 wt.% Rh, S2 = 3.7 wt.% Rh (S:C = 1.0; 1 atm; 27 ms contact time).

It was somewhat counter-intuitive that the catalyst with the higher Rh loading (S1) would deactivate at a faster rate and perform somewhat less favorably than the catalyst with the lower catalyst loading (S2). A possible explanation for this apparent anomaly was not readily apparent until after extensive microstructural analysis had been performed (results previously discussed). The explanation, then for the difference in performance between the two specimens was found in their microstructures. The S2 specimen, composed of smaller Rh catalyst particles, and lower in concentration, proved to have not only a higher initial light-off activity, but also had better sustained performance and deactivated less than the S1 catalyst with higher Rh loading (larger, more numerous Rh particles). Apparently, the higher concentration of Rh particles on the surface of the alumina grains facilitated relatively enhanced sintering of the Rh metal, which subsequently lead to the

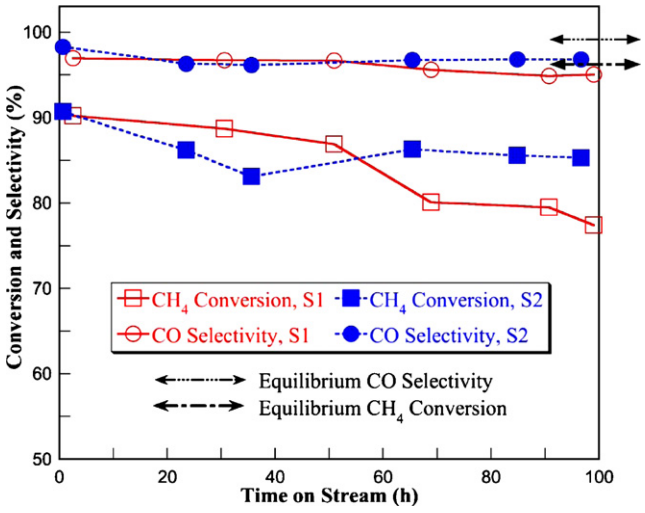

Fig. 7. Time-on-stream CH_4 conversion and CO selectivity for engineered Rh-porous alumina catalytic shims; S1 = 10 wt.% Rh, S2 = 3.7 wt.% Rh (900 °C, S:C = 1.0, 1 atm, 27 ms contact time).

increased deactivation of that catalyst. Additional experiments are planned to seek ways to minimize Rh sintering as a strategy to minimize deactivation.

Although coking was initially suspected as a possible cause for the slight deactivation observed, no evidence of coking was found. In fact, it is very important to point out that there was no coke deposition observed on the surface of either S1 or S2 spent catalysts, even under the demanding SMR testing conditions of S:C = 1.0. Coke is readily observable visually on tested catalysts as black soot. In an SEM, the coke is easily imaged due to its relatively low electron yield and thus appears black and fibrous. In the TEM, coke can often be imaged as nanowires. None of these features were observed in either of the specimens. Not only was there no microstructural evidence for coke formation on these catalysts, but there was no operational evidence for coke formation either. Carbon balance calculations for both specimens during the 100 h TOS tests yielded a value of 0% – all of the carbon introduced as methane was accounted for by production of CO and CO_2. The formation of coke in a microchannel reactor bed is often accompanied by a large increase in the pressure drop across the bed. However for both S1 and S2 there was only a nominal pressure drop across the microchannel bed during testing. The conclusion was that these catalysts proved to perform coke-free under the stated operating conditions. The implication is that application of ceramic-based catalyst supports may allow the SMR reactions to be operated at lower S:C ratios without problems of coke formation, thus improving reactor efficiency and lower energy costs.

4. Conclusions

Engineered, porous, ceramic support shims directly dispersed with Rh were specifically designed to address three material limitations encountered with wash-coated, metal-based, catalyst supports: metal support corrosion, catalyst carrier powder delamination from the metal support, and catalyst carrier powder sintering. Additionally, it was desired to demonstrate high-performance, coke-resistant, SMR activity with these engineered catalysts. Each of these objectives has been demonstrated with the engineered catalysts based on the engineered, tape cast, porous, alumina shims. The porous alumina substrate was thermodynamically stable under the corrosive and hydrothermal conditions characteristic of SMR reactions. In particular, the porous, thermodynamically stable alpha-phase alumina support did not sinter or degrade under the testing conditions. Since there is no wash coating involved with the engineered catalyst, the wash coat delamination issue was eliminated. Two different catalyst loadings were studied on these porous ceramic supports, and both achieved near equilibrium conversions and selectivities, and only deactivated slightly over the 100 h test. The difference in catalytic performance between the two specimens was correlated to differences in microstructure. The greater deactivation associated with the higher Rh loading was attributed to sintering of the catalyst due to shorter diffusion distances between the particles. There was no evidence of coke formation on either spent catalyst, indicating the coke-resistant attributes of these supports. Application of these highly active, engineered catalyst supports is projected to result in improved SMR reaction efficiencies and lower operational costs due to their ability to operate at lower S:C ratios.

Acknowledgements

The authors would like to gratefully acknowledge the contributions of the following individuals who assisted in this work: James Martinez and Jarrod Crum.

This work was funded by laboratory directed research and development funds at Pacific Northwest National Laboratory. Portions of it were performed in the Environmental Molecular Science Laboratory, a national scientific user facility sponsored by the U.S. Department of Energy's Office of Biological and Environmental Research and located at Pacific Northwest National Laboratory in Richland, WA. Pacific Northwest National Laboratory is operated by Battelle for the Department of Energy under contract DE-AC06-76RLO 1830.

References

[1] A.L.Y. Tonkovich, Y. Wang, in: Y. Wang, J.D. Holladay (Eds.), Microreactor Technology and Process Intensification, vol. 914 of the ACS Symposium Series, American Chemical Society, Washington, DC, 2005 , p. 47.

[2] Y. Wang, B.R. Johnson, J. Cao, Y.-H. Chin, R.T. Rozmiarek, Y. Gao, A.L. Tonkovich, in: Y. Wang, J.D. Holladay (Eds.), Microreactor Technology and Process Intensification, vol. 914 of the ACS Symposium Series, American Chemical Society, Washington, DC, 2005, p. 102.

[3] J.L. Zilka-Marco, A.L.Y. Tonkovich, M.J. LaMont, S.P. Fitzgerald, D.P. VanderWiel, Y. Wang, R.S. Wegeng, IMRET 4: Fourth International Conference on Microreaction Technology, Atlanta, GA, March 5–9, (2000), p. 301.

[4] M.K. Drost, C. Call, J. Cuta, R. Wegeng, Microscale Therm. Eng. 1 (1997) 321.

[5] D.P. VanderWiel, J.L. Zilka-Marco, Y. Wang, A.Y. Tonkovich, R.S. Wegeng, IMRET 4: Fourth International Conference on Microreaction Technology, Atlanta, GA, March 5–9, (2000), p. 187.

[6] A.Y. Tonkovich, J.L. Zilka, M.J. LaMont, Y. Wang, R.S. Wegeng, Chem. Eng. Sci. 54 (1999) 2947.

[7] E.A. Daymo, D.P. VanderWiel, S.P. Fitzgerald, Y. Wang, R.T. Rozmiarek, M.J. LaMont, A.Y. Tonkovich, IMRET 4: Fourth International Conference on Microreaction Technology, Atlanta, GA, March 5–9, (2000), p. 364.

[8] S.P. Fitzgerald, R.S. Wegeng, A.Y. Tonkovich, Y. Wang, H.D. Freeman, J.L. Marco, G.L. Roberts, D.P. VanderWiel, IMRET 4: Fourth International Conference on Microreaction Technology, Atlanta, GA, March 5–9, (2000), p. 358.

[9] W.E. TeGrotenhuis, R.S. Wegeng, D.P. VanderWiel, G.A. Whyatt, V.V. Viswanathan, K.P. Schielke, G.B. Sanders, T.A. Peters, IMRET 4: Fourth International Conference on Microreaction Technology, Atlanta, GA, March 5–9, (2000), p. 343.

[10] D.L. King, K. Brooks, C. Fischer, L. Pederson, G. Rawlings, V.S. Stenkamp, W. TeGrotenhuis, R. Wegeng, G. Whyatt, in: Y. Wang, J.D. Holladay (Eds.), Microreactor Technology and Process Intensification, vol. 914 of the ACS Symposium Series, American Chemical Society, Washington, DC, 2005, p. 119.

[11] J.D. Holladay, E.O. Jones, R.A. Dagle, G.G. Xia, C. Cao, Y. Wang, in: Y. Wang, J.D. Holladay (Eds.), Microreactor Technology and Process Intensification, vol. 914 of the ACS Symposium Series, American Chemical Society, Washington, DC, 2005, p. 162.

[12] D.R. Palo, J.D. Holladay, R.A. Dagle, Y.-H. Chin, in: Y. Wang, J.D. Holladay (Eds.), Microreactor Technology and Process Intensification, vol. 914 of the ACS Symposium Series, American Chemical Society, Washington, DC, 2005, p. 209.
[13] K.P. Brooks, J.M. Davis, C.M. Fischer, D.L. King, L.R. Pederson, G.C. Rawlings, V.S. Stenkamp, W. TeGrotenhuis, R.S. Wegeng, G.A. Whyatt, in: Y. Wang, J.D. Holladay (Eds.), Microreactor Technology and Process Intensification, vol. 914 of the ACS Symposium Series, American Chemical Society, Washington, DC, 2005, p. 238.
[14] M.K. Drost, R.S. Wegeng, P.M. Martin, K.P. Brooks, J.L. Martin, C.J. Call, IMRET 4: Fourth International Conference on Microreaction Technology, Atlanta, GA, March 5–9, (2000), p. 308.
[15] W.E. TeGrotenhuis, R.J. Cameron, V.V. Viswanathan, R.S. Wegeng, IMRET 3: Third International Conference on Microreaction Technology, Frankfurt, Germany, 1999.
[16] D.W. Matson, P.M. Martin, A.L.Y. Tonkovich, G.L. Roberts, Micromachined Devices and Components IV, Proceedings of SPIE, vol. 3514, Santa Clara, CA, September, (1998), p. 386.
[17] W. Wang, S.M. Stagg-Williams, F.B. Noronha, L.V. Mattos, F.B. Passos, Catal. Today 98 (2004) 553.
[18] J. Cao, J. Hu, T. Mazanec, Y. Wang, IMRET: Eighth International Conference on Microreaction Technology, 2005 AIChE Spring National Meeting Conference Proceedings, Atlanta, GA, (2005), p. 2943.
[19] J.D. Holladay, Y. Wang, E. Jones, Chem. Rev. 104 (2004) 4767.
[20] Y. Wang, Y.H. Chin, R.T. Rozmiarek, B.R. Johnson, Y. Gao, J. Watson, A.Y.L. Tonkovich, D.P. VanderWiel, Catal. Today 98 (2004) 575.
[21] R.E. Mistler, E.R. Twiname, Tape Casting: Theory and Practice, American Ceramic Society, Westerville, OH, 2000, p. 298.
[22] J.S. Reed, Principles of ceramic processing, John Wiley & Sons, New York, 1995.
[23] D.B. Williams, B.C. Carter, Transmission Electron Microscopy: A Textbook for Materials Science, Plenum Press, New York, 1996, p. 729.
[24] J.I. Goldstein, D.E. Newbury, P. Echlin, D.C. Joy, A.D. Romiq Jr., C.E. Lyman, C. Fiori, E. Lifshin, Scanning Electron Microscopy and X-ray Microanalysis: A Text for Biologists, Materials Scientists, and Geologists, Plenum Press, New York, 1992, p. 820.